TWO-DIMENSIONAL (2D) NANOMATERIALS FOR BIOMEDICAL APPLICATIONS

An Undergraduate Research Scholars Thesis

by

JAMES L. GENTRY

Submitted to the Undergraduate Research Scholars program
Texas A&M University
in partial fulfillment of the requirements for the designation as an

UNDERGRADUATE RESEARCH SCHOLAR

Approved by
Research Advisor: Dr. Akhilesh Gaharwar

May 2016

Major: Biomedical Engineering

TABLE OF CONTENTS

ABSTRACT

Two-Dimensional (2D) Nanomaterials for Biomedical Applications

James L. Gentry
Department of Biomedical Engineering
Texas A&M University

Research Advisor: Dr. Akhilesh Gaharwar
Department of Biomedical Engineering

As regenerative medicine progresses, the need for non-cytotoxic and bioactive tissue scaffolds becomes increasingly urgent. To address this need, a PEG-based hydrogel crosslinked by molybdenum disulfide (MoS_2) nanoassemblies was developed. The 2D nanoflakes that form these assemblies are rich with defects, specifically elemental vacancies, that easily conjugate thiolated ligands. MoS_2 has been extensively studied for application in electrochemistry, nanoelectronics, lubricants, and biosensing, yet studies describing their role in the biomedical field are rare. Using a multi-arm PEG-thiol, this defect-mediated reaction is exploited to form a mechanically stiff hydrogel. By varying reactant ratios, several samples of MoS2 nanoassemblies have been synthesized using a hydrothermal method. The structure and defect content of each sample was characterized to determine the optimal nanoassembly for gelation. This work discusses the chemical and morphological characterizations and the mechanical properties of the developed PEG-MoS_2 gels. The physiologically relevant properties and behavior of the hydrogel indicate that it is suitable for further exploration in tissue engineering applications.

DEDICATION

I would like to dedicate this thesis to my family. You have encouraged and supported me through this entire endeavor even when it was an inconvenience to you. I appreciate all that you have sacrificed for me.

ACKNOWLEDGMENTS

I would like to thank Dr. Manish Jaiswal and Dr. Akhilesh Gaharwar for their support and advice with this project. Without their input and help, I doubt this work would have been as successful as it has been.

I would also like to thank C. W. Peak and Lauren Cross who have taught me much about biomaterials and their application in cell culture. Their knowledge has been invaluable for the accomplishment of this thesis.

CHAPTER I

INTRODUCTION

Biomaterials

Biomaterials are integral in designing methods that repair or replace the function of a tissue or organ that has been damaged or removed. In order to fulfill their important role, all biomaterials need to have a few fundamental properties: biocompatibility, stability in physiological conditions, and fast and easy production. Except for these, biomaterials can have a wide array of properties; depending on their application, biomaterials can be hydrophilic or hydrophobic, mechanically strong or weak, biodegradable or non-biodegradable [1]. Therefore, the properties of one biomaterial can be completely different from those of another. Since there is a need for so many materials that have many varying properties, a base material that can be tuned to exhibit varying properties is needed. Fortunately, one class of biomaterial, namely polymeric hydrogels, is easily modified to exhibit a myriad of properties without having to change the basic composition of the material. As seen in *Figure 1*, hydrogels are created by either chemically or physically crosslinking individual polymer strands to one another, creating a three-dimensional interconnected polymer network [1]. Hydrophilic by definition, hydrogels swell with water to create a soft, flexible material that closely mimics the microenvironment of many tissues found in the body. They are often used to mimic complex tissue architecture due to their structural, chemical, electrical, and biological properties [2]. Despite their favorable innate properties, hydrogels must be further modified in order to enhance their biomimetic properties. If these networks are to fully support and encourage specialized tissue growth or regeneration, they must closely mimic conditions found in specific areas of the body.

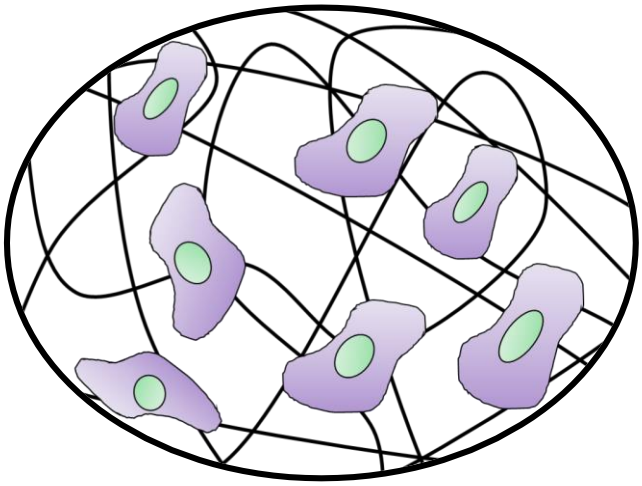

Figure 1. Polymeric hydrogel tissue scaffold. Cells are seen proliferating on the crosslinked polymer strands that form the hydrogel structure, as represented by the black lines.

Modification of hydrogels

Hydrogels can be modified through polymer functionalization, block copolymerization, and graft copolymerization. Adding functional groups to a polymer can create versatile properties (Table 1). Polymerizing one or more species of monomer with a base monomer creates a copolymer. Block copolymers alternate between many repeated units of different species of monomer. In graft copolymers, chains of polymer species branch from a strand of a single polymer species. Copolymerization often creates a hydrogel with emergent properties that can be used for biomedical applications (Table 2). An illustration of all these polymerization types can be seen in *Figure 2*.

Table 1. Added functionality.

Base Polymer	Functional Group	Added Functionality
PEG	Acrylate	UV-induced gelation
Gelatin	Methacrylate	UV-induced gelation
PEG	Thiol	Click chemistry
PEG	Azide	Click chemistry

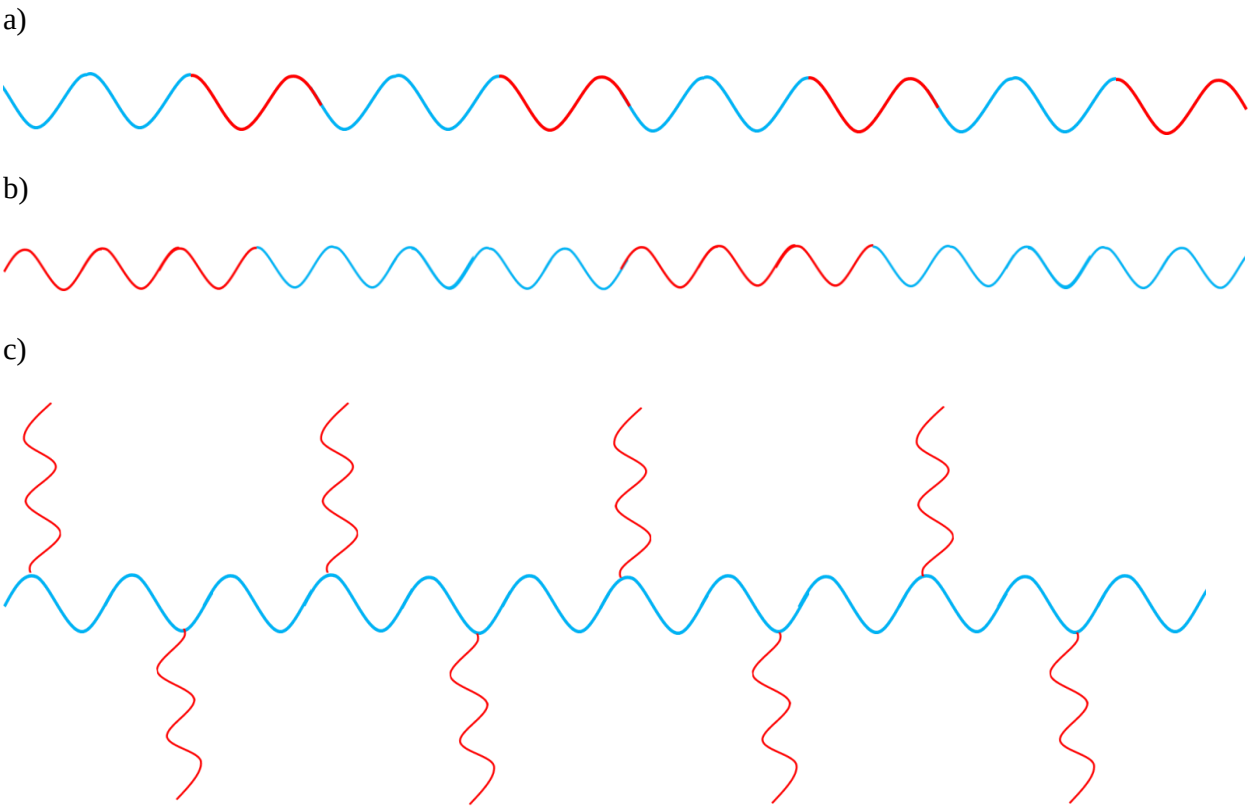

Figure 2. Copolymerization types. a) An alternating copolymer is shown with the blue unit representing one monomer species and the red unit representing another. b) A block copolymer is shown with many red units alternating with many blue units. c) A graft copolymer is shown with red units grafted to a blue polymer backbone.

Nanocomposite hydrogels

Yet another way to tune the properties of a hydrogel is to incorporate nanoparticles into the polymer matrix. Nanoparticles can be chemically integrated into the network, or they can be physically dispersed in the matrix. The incorporation of nanomaterials into hydrogel networks has been shown to create unique properties within the hydrogel: nanosilicates have spontaneously induced osteogenic differentiation of preosteoblasts [3]; gold nanoparticles create electrically conductive systems [2]; a graphene derivative increased tensile strength of a hydrogel by 900% [2].

Two-dimensional nanoparticles

Recently, graphene-like 2D layered nanomaterials, including transition metal dichalcogenides monolayers (TMDCs), boron nitride nanosheets, and graphite-carbon nitride nanosheets, have received much attention in the biomedical field due to their unique properties [4]. Their structural and electronic properties make them ideal candidates for use in next-generation bio-optical sensing and bioelectronics systems. Their chemical, catalytic, and non-cytotoxic properties will allow for greatly enhanced therapeutics through nanomedicine, smart drug delivery systems, and improved diagnostic tests [4].

Molybdenum disulfide (MoS_2)

Of these layered nanomaterials, molybdenum disulfide (MoS_2) is arguably the most studied. *Figure 3a* illustrates the structure of a MoS_2 nanosheet. There are two MoS_2 nanosheet phases: the metallic 1T polytype and the semiconducting 2H polytype. The unit structures of the 2H-MoS_2 and 1T-MoS_2 crystal lattice, seen in *Figures 3b and 3c* respectively, differ only by a

rotation of the lower sulfur atoms by 60 degrees. The effect of this rotation on the structure of the nanosheet is depicted in the top views of 2H-MoS_2 and 1T-MoS_2 (*Figures 3d and 3e*).

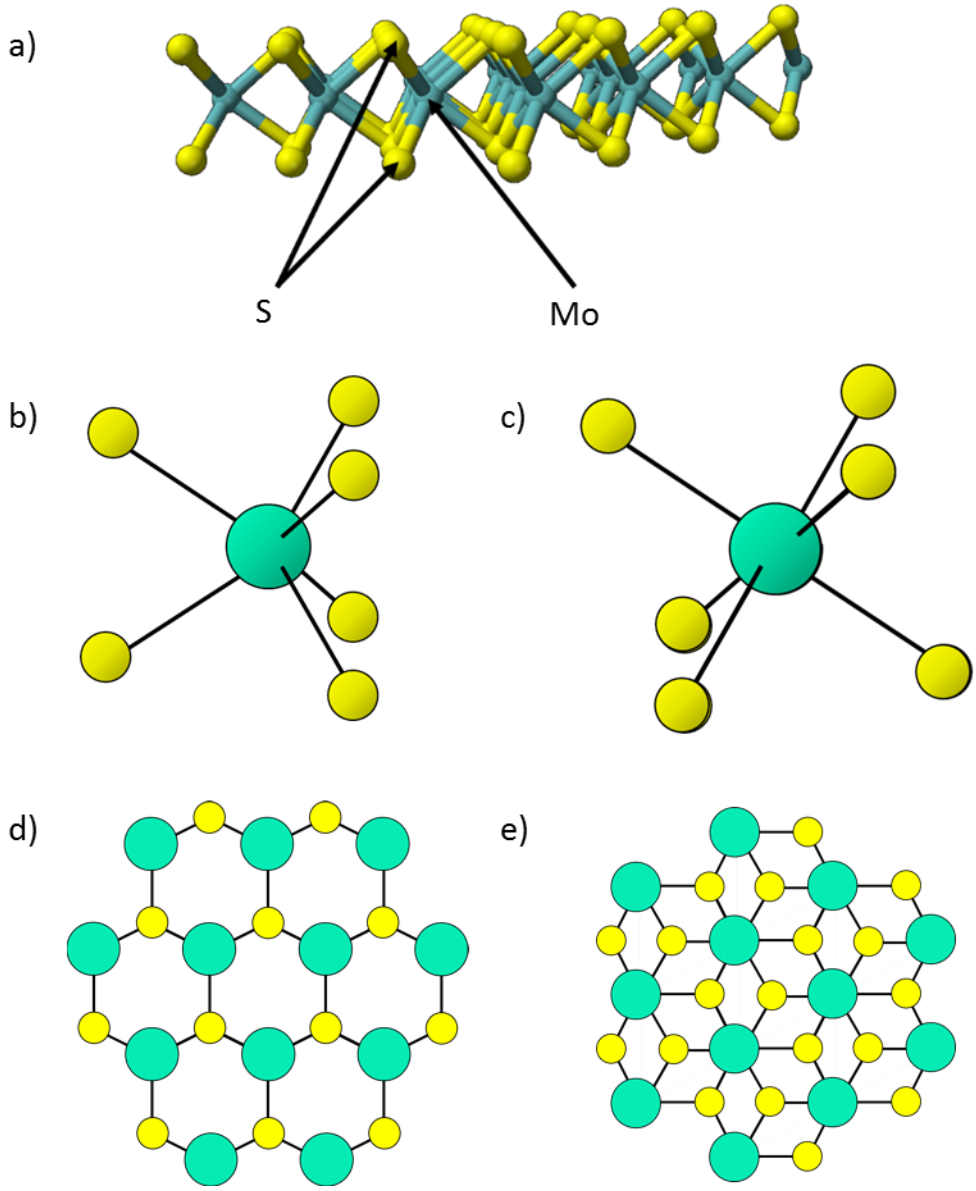

Figure 3. MoS_2 crystal structure. a) A single layer of a MoS_2 nanosheet is depicted. b) and c) The unit cell structure of 2H- and 1T-MoS_2 are shown respectively. d) and e) The top view of 2H- and 1T-MoS_2 nanosheets are shown respectively.

MoS_2 has many properties that are well-suited for biomedical application. It has been found to have low cytotoxicity and good biocompatibility [5]. MoS_2 nanosheets have been determined to be effective drug carriers due to their high drug loading capacity and excellent stability in physiological conditions. The same studies exploited MoS_2's photothermal reactivity with near-infrared light in order to locally ablate cancer cells instead of attacking the disease through a system-wide procedure [6, 7]. Studies have shown that MoS_2 can be easily conjugated with thiol-terminated polymers, which further enhances its utility in designing biocompatible and stable systems [8, 9]. However, there has been no attempt at integrating these nanosheets into a hydrogel network for eventual application as a tissue scaffold.

As mentioned above, MoS_2 easily conjugates with thiol-terminated polymers. Defects throughout the MoS_2 nanosheet structure are repaired by filling the sulfur vacancies on the surface with the sulfur atom of the thiol group [6, 7, 10-13]. Additionally, molybdenum vacancies may allow the formation of a disulfide bond between a free sulfur and thiol group. This thiol-MoS_2 interaction may be utilized to form a hydrogel network. Again, a hydrogel forms when different polymer strands are either chemically or physically crosslinked to one another, creating a polymer network [1]. Therefore, the MoS_2 nanosheets may act as chemical crosslink epicenters for a thiolated polymer through defect-mediated interactions. This work describes the properties and behavior of a PEG-based hydrogel crosslinked by this hypothesized process.

CHAPTER II

METHODS

Hydrothermal synthesis of MoS_2

The synthesis of defect-rich MoS_2 was adapted from a previous study describing a method to introduce defects into MoS_2 [14]. In 35 mL of ultrapure water, 1 mmol of hexaamonium heptamolybdate tetrahydrate (7 mmol of molybdenum) and 30 mmol of thiourea (30 mmol of sulfur) were stirred until a homogeneous solution was obtained. The solution was heated at 220°C in a Teflon-coated autoclave for 6 hours. The product was allowed to cool to room temperature, was washed with water and ethanol several times, and was dried under vacuum at 50°C. To determine the effect of reaction time on nanoassembly morphology, this entire process was repeated twice for 6 hours and 30 hours respectively. To determine the effect of thiourea on amount and type of defects, thiourea concentration was varied across four other syntheses while reaction time remained constant at 18 hours.

Characterization of MoS_2

Scanning electron microscopy (SEM)

A thin film was deposited on a silica substrate using the drop cast method. The sample was sputter coated with Au/Pd up to a thickness of 8nm before being mounted onto the imaging stage. SEM images were obtained using a FEI Quanta 600 at 20 kV.

Transmission electron microscopy (TEM)

A thin film was deposited on a silica substrate using the drop cast method. TEM images were obtained using a JEOL JEM-2010 (Japan) at an accelerating voltage of 200 kV on a carbon grid.

X-Ray powder diffraction (XRD)

XRD spectra were obtained using a Bruker powder diffractometer.

Raman spectroscopy

Raman spectra were found by exciting the samples at 532 nm by a green laser.

X-Ray photoelectron spectroscopy (XPS)

The binding energies of Mo and S were analyzed using an Omicron XPS/UPS system with Argus detector. The raw data were processed and deconvoluted by CasaXPS multiple peak fit software version 2.3.15.

Zeta potential

A dilute dispersion of MoS_2 nanoassemblies in ultrapure water was prepared. The zeta potential of the nanoassemblies are measured at 25 °C using a Zetasizer (Malvern Instrument, U.K.) equipped with a He−Ne laser.

Ultraviolet-Visible (UV-Vis) spectroscopy

Spectra were obtained using a Tecan Infinite® M200 Pro equipped with a UV Xenon light source.

Photoluminescence (PL) spectroscopy

Dilute solutions of MoS_2 nanoassemblies in ultrapure water were prepared. Photoluminescence spectra were found by exciting the samples at 470 nm.

Preparation of hydrogel

To prepare the nanocomposite hydrogels, the defect-rich MoS_2 (0.25, 0.50, 1.00, 2.00 wt %) was dispersed in ultrapure water and sonicated for 4 hours. PEG-SH (10 wt. %) was dissolved in this dispersion and injected into sheet molds. In order to keep the MoS_2 dispersed throughout the solution, a magnetic stir bead was placed in the mold as well, and the solution in the mold was stirred continuously until gelation occurred. The nanocomposites sat for 24 hours to ensure maximum crosslinking, were removed from the molds, and were soaked in 1X PBS or ultrapure water for 24 hours.

Characterization of hydrogel

Scanning electron microscopy (SEM)

The hydrogel was kept in -80°C freezer for 8 hrs and was subsequently lyophilized for 48 hrs. The dry gel was cut transversely to expose the micropore structure for imaging. The sample was sputter coated with Au/Pd up to a thickness of 8nm before being mounted onto the imaging stage. SEM images and EDS maps were obtained using a FEI Quanta 600 at 20 kV fitted with Oxford EDS system.

Uniaxial compression testing

Cylindrical gels were punched from the hydrogel sheet using a 5 mm biopsy punch. Using an ADMET Xpert 7600 mechanical tester, the gels were loaded at a rate of 1 mm/min until a strain of 50% was reached and were unloaded at a rate of -1 mm/min until a strain of 0% was reached. This process was repeated for total of 5 cycles. The compressive modulus was calculated from the slope of the linear elastic region corresponding to 0.05−0.20 strain in the engineering stress−strain curve (force divided by original cross-sectional area).

Rheological testing

Cylindrical gels were punched from the hydrogel sheet using a 10 mm biopsy punch. Measurements were taken using a 10 mm flat geometry on an Anton Paar model MCR 301 at a gap of 1 mm. Specific shear stress and oscillatory stress values are described in Results section.

CHAPTER III

RESULTS

A nanocomposite hydrogel composed of thiolated multi-arm PEG and MoS_2 nanoassemblies was developed. Reaction conditions were varied to create multiple samples of defect-rich MoS_2 nanoassemblies. These nanoassemblies were characterized to determine their potential as crosslinking agents. The MoS_2 nanoassemblies best-suited for crosslinking were dispersed in water, and 4-arm PEG-SH was dissolved in the dispersion. Spontaneous crosslinking through the mechanism shown in *Figure 4* took place over the course of a few days. The mechanical properties of the resulting hydrogel were subsequently investigated.

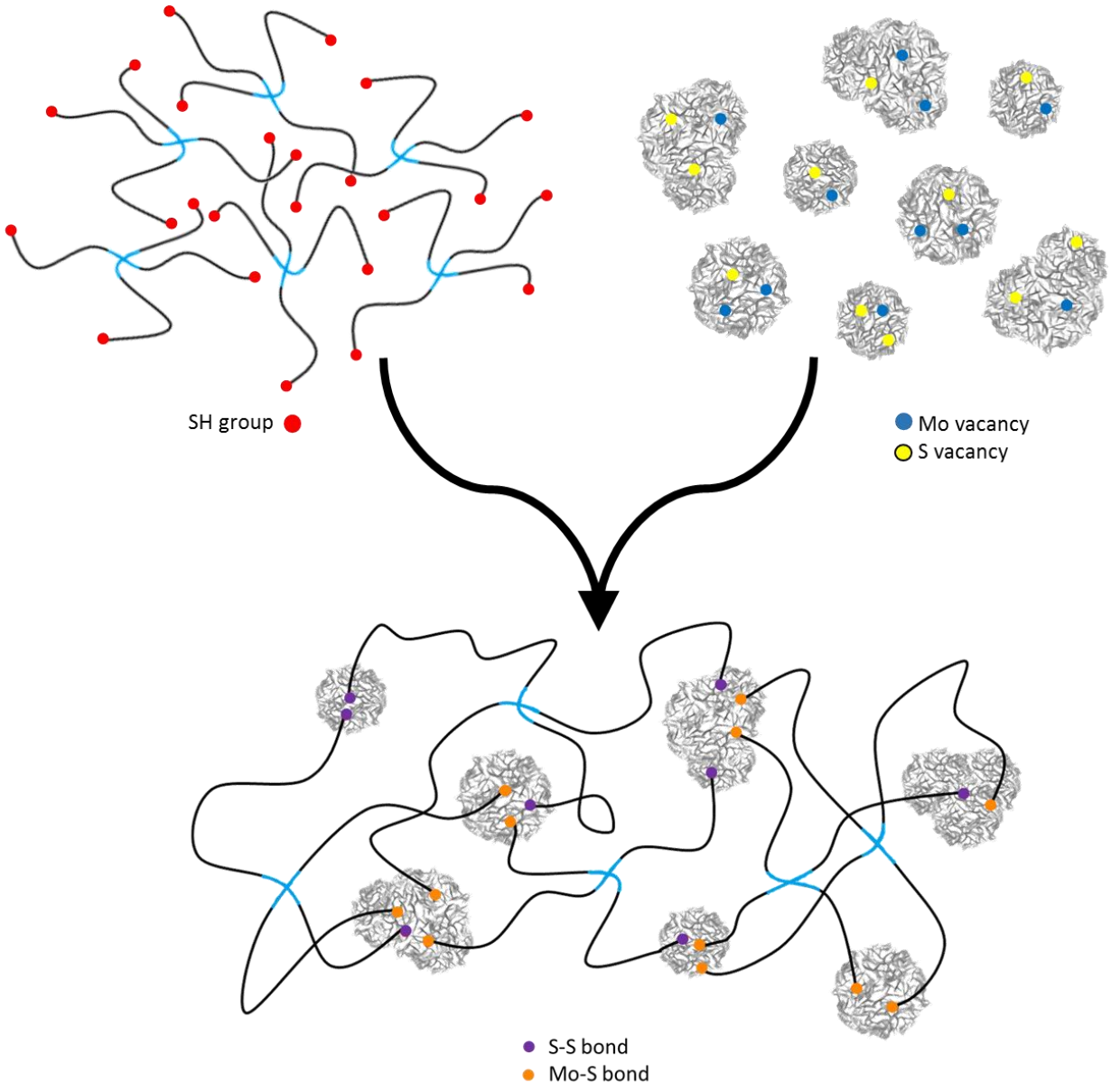

Figure 4. Proposed gelation mechanism. The defects in MoS_2 are sites for thiol conjugation. Multi-arm, terminally thiolated polymers can be crosslinked via this conjugation, resulting in a mechanically stiff hydrogel.

MoS_2 characterization

Imaging

Varying the reaction conditions of the MoS_2 nanoassemblies created morphological differences between the samples. As seen in *Figure 5a*, increasing reaction time increased nanoassembly size and promoted "petal" development. Reaction time past 18 hours did not cause a significant change in nanoassembly morphology, so the remaining nanoassembly compositions were synthesized for 18 hours. As seen in *Figure 5b*, nanoassembly size and "petal" development increased as a result of increasing sulfur precursor concentration.

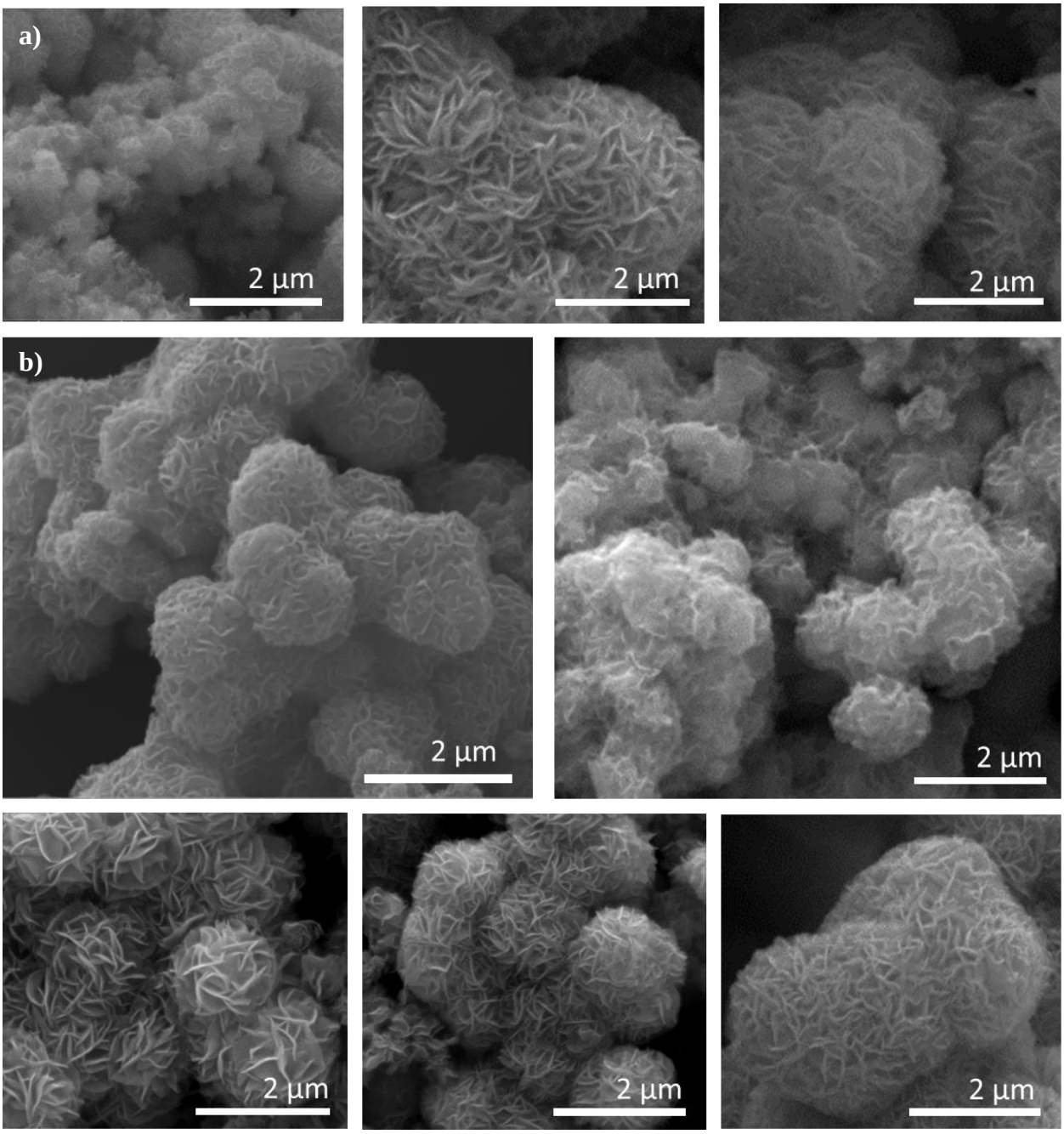

Figure 5. Defect-rich MoS_2 nanoassembly morphology via SEM imaging. a) The MoS_2 nanoassemblies with reaction times of 6h, 18h, and 30h are depicted from left to right. b) The MoS_2 nanoassemblies with varying precursor molar ratios of molybdenum to sulfur are presented. The middle row depicts 1:1 and 1:2 precursor molar ratio MoS_2, and the bottom row depicts 1:3, 1:4, and 1:6 precursor molar ratio MoS_2 from left to right.

A nanoassembly composed of many petal-like nanosheets can be seen in *Figure 6*. These rippled, thin structures are ideal for crosslinking due to their large surface area to volume ratio; the thiol groups can easily conjugate at the many exposed vacancy sites.

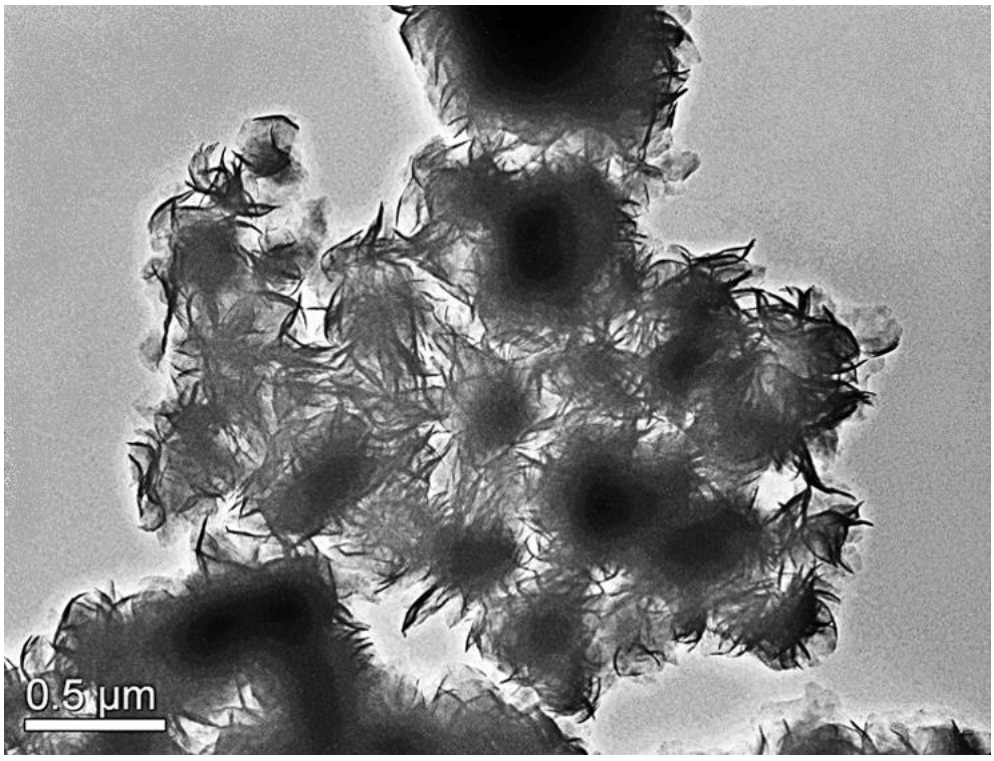

Figure 6. Defect-rich MoS_2 nanoassembly morphology via TEM imaging. 1:4 MoS_2 nanoassemblies are presented.

Structural characterization

Figure 7a depicts the XRD patterns of each composition of nanoassembly. The peaks confirm that the nanoassemblies are predominantly composed of the polytype 2H-MoS_2. The rings of the selected area electron diffraction (SAED) depicted in the inset correspond to the peaks of the XRD pattern, further validating the presence of 2H-MoS_2. *Figure 7b* depicts the Raman spectra of each composition of nanoassembly. The peaks labeled E^1_{2g} and A_{1g} indicate the presence of

2H-MoS_2, and the peaks labeled J_2, E_{1g}, and J_3 indicate the presence of 1T-MoS_2. As thiourea concentration increases, the 2H polytype becomes more prominent, and the 1T polytype becomes less so. This trend is also seen in the XRD data; as the thiourea concentration increases, a characteristic plane of 2H-MoS_2 (006) becomes increasingly prominent. The XPS data presented in *Figure 7c* verifies the chemical composition of 1:4 MoS_2.

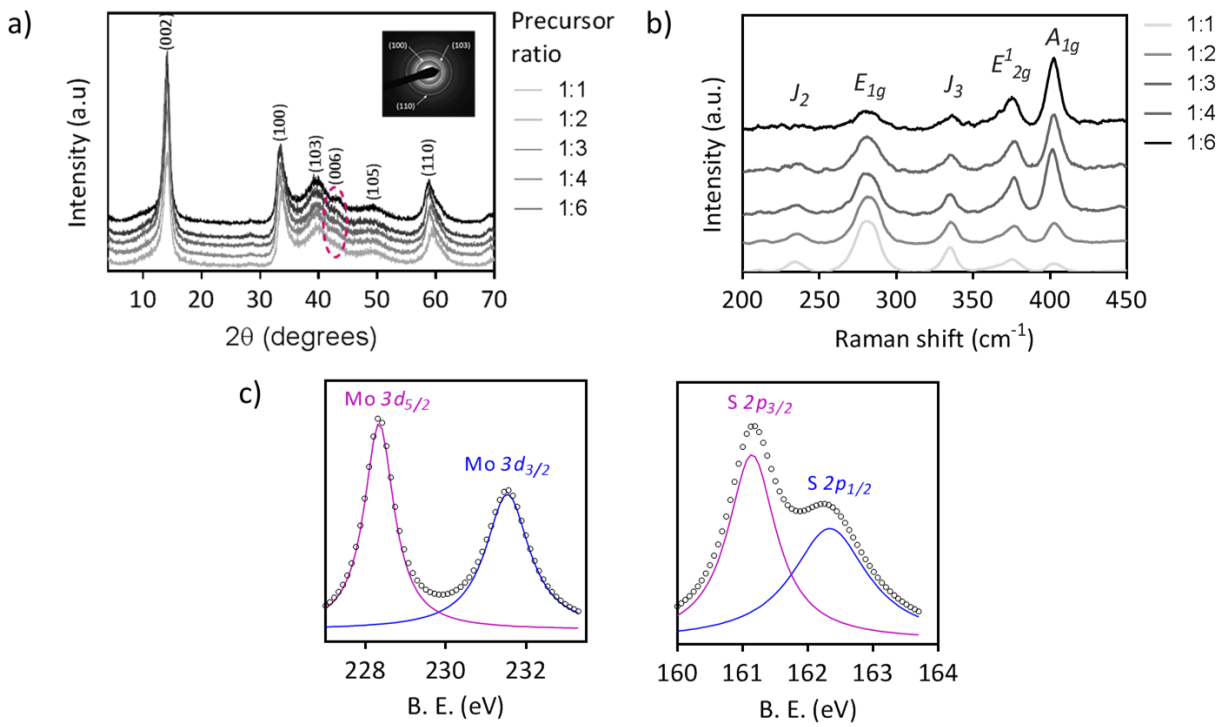

Figure 7. Structural characterization of MoS_2 nanoassemblies. a) The XRD patterns of the MoS_2 nanoassemblies are presented along with the SAED pattern of 1:4 MoS_2. b) Raman spectra of the MoS_2 nanoassemblies depicting the characteristic peaks of 2H- and 1T- MoS_2 are presented. c) XPS data of 1:4 MoS_2 is presented.

As depicted in *Figure 8*, the Zeta potential of the nanoassemblies was -37.5 mV (±7.5 mV).

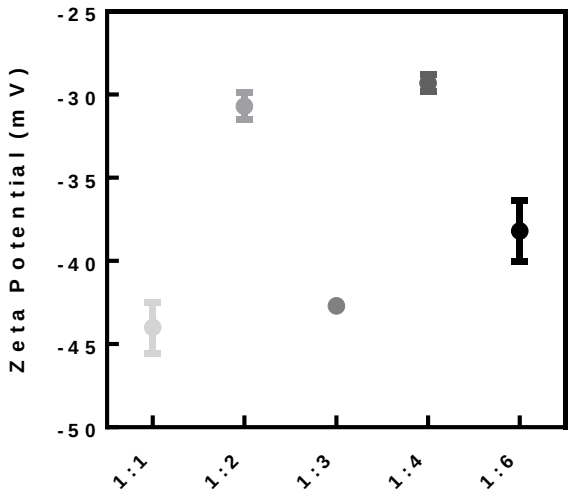

Figure 8. Surface properties of MoS_2 nanoassemblies. Zeta potential is presented.

Defect Characterization

The type and relative amount of defects in each composition of nanoassembly were determined through photoluminescence (PL) and Raman spectroscopy. Oxygen physically adsorbs to the defects in MoS_2 [15]. When exposed to light of a certain wavelength, this interaction causes the emittance of light. To determine the wavelength of light needed to excite the MoS_2, UV-Vis absorbance was determined for each composition of MoS_2 nanoassemblies. As seen in *Figure 9a*, all compositions absorbed light of wavelengths 470, 610, and 660 nm. Photoluminescence experiments of each composition was run at 470 nm. *Figure 9b* shows three major emission peaks across all compositions. Except for 1:3 MoS_2, emission intensity increases as thiourea concentration increases, indicating the creation of defects in all but the 1:3 composition. Since 1:3 MoS_2 does not fit the aforementioned trend, it is believed that the type of defects in 1:4 and

1:6 MoS_2 differ from those in 1:1 and 1:2 MoS_2. The Raman peaks E^1_{2g} and A_{1g}, which represent in-plane and out-of-plane vibrations of S with respect to Mo respectively, are presented in *Figure 9c*. *Figure 9d* shows an increase of out-of-plane vibrations for every in-plane vibration as thiourea concentration increases. High out-of-plane vibrations indicate a high level of S atoms (or a low level of S vacancies); as thiourea concentration increases, the relative number of sulfur defects decreases. Therefore, 1:1 and 1:2 MoS_2 have sulfur vacancies as indicated by their low out-of-plane S vibrations. Since the Raman data does not describe Mo behavior, the appearance of Mo vacancies in any composition cannot be directly determined. However, as the PL data indicates many defects in 1:4 and 1:6 MoS_2, and the Raman data shows few sulfur vacancies, the defects in 1:4 and 1:6 MoS_2 must be Mo vacancies.

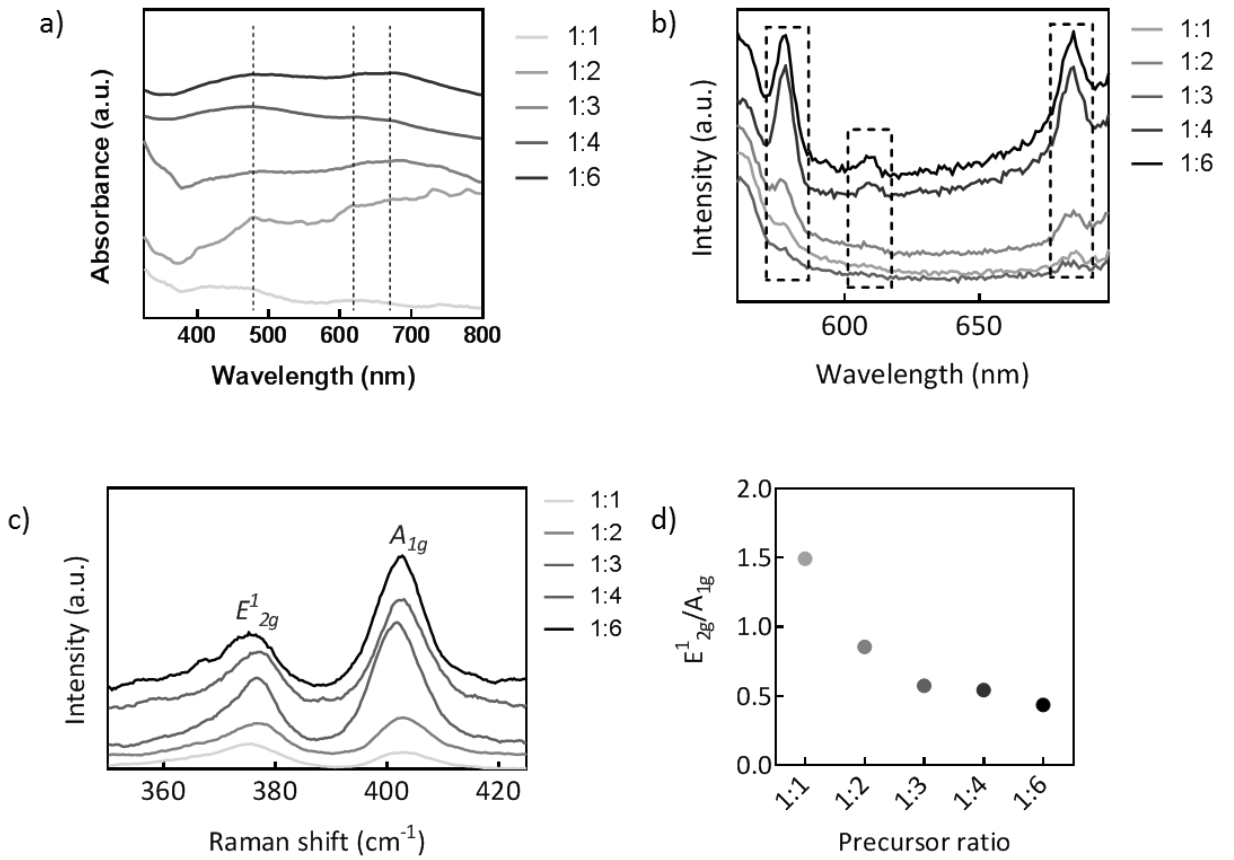

Figure 9. Defect characterization of MoS_2 nanoassemblies. a) Absorption peaks at 470, 610, and 660 nm are depicted on the UV-Vis absorption spectra. b) PL spectra of MoS_2 nanoassemblies are depicted. c) Raman spectra of MoS_2 nanoassemblies depicting the 2H- MoS_2 characteristic peaks are presented. d) The ratio of sulfur in-plane vibrations to out-of-plane vibrations is presented.

MoS_2 Optimization

These characterizations were performed to determine the optimal defect-rich MoS_2 for the crosslinking of PEG-SH. 1:3 MoS_2 had relatively few defects as shown by the PL data, so it would be difficult to use as a crosslinking agent. 1:1 and 1:2 MoS_2 were composed of high levels of 1T-MoS_2; since 2H-MoS_2 is the most-studied polytype, compositions containing 1T-

MoS_2 were not considered for use. Both 1:4 and 1:6 MoS_2 were deemed optimal due to their similar properties (high level of defects and 2H-MoS_2 composition), but 1:4 was chosen for further experimentation due to its smaller size and its less-expensive synthesis.

Hydrogel characterization

Crosslink characterization

To determine if MoS_2 played a role in the crosslinking of a PEG-SH hydrogel, the gelation kinetics of both PEG-SH solution and PEG-SH/MoS_2 solution were monitored by measuring the storage modulus over time. In ultrapure water, a 10 wt. % PEG-SH solution never crosslinked into a hydrogel. To prepare a PEG-SH/MoS_2 solution, the MoS_2 was first sonicated for 4 hrs in ultrapure water (2 wt. %). PEG-SH was added to the dispersion (10 wt. %) and stirred for 18 hrs until the solution became viscous. The solution was then analyzed by the rheometer at constant oscillation (1 Hz) and stress (1 Pa). As seen in *Figure 10a*, the storage modulus plateaued at approximately 2.5 kPa after a total of 23 hrs, indicating that MoS_2 has some role in PEG-SH gelation. Since this hydrogel will be used in cell culture, the gelation kinetics of PEG-SH and PEG-SH/MoS_2 in cell culture media were determined. PEG-SH solution was analyzed by the rheometer 2 hours after preparation to minimize the effects of desiccation. The storage modulus of the solution plateaued after a total of 4 hrs (*Figure 10b*). Gelation most likely occurred through oxidation of thiol groups by disulfide-containing amino acids. To prepare a PEG-SH/MoS_2 solution in media, the MoS_2 was first sonicated for 4 hours in media (2 wt. %). PEG-SH was added to the dispersion (10 wt. %), and the solution was immediately analyzed by the rheometer. The storage modulus of the solution plateaued after 1 hour, a significant reduction compared to gelation time in water (*Figure 10c*). However, since gelation occurred without

MoS_2 in media, the exact crosslinking mechanism is unknown. Therefore, hydrogels used in all subsequent experiments were crosslinked in ultrapure water.

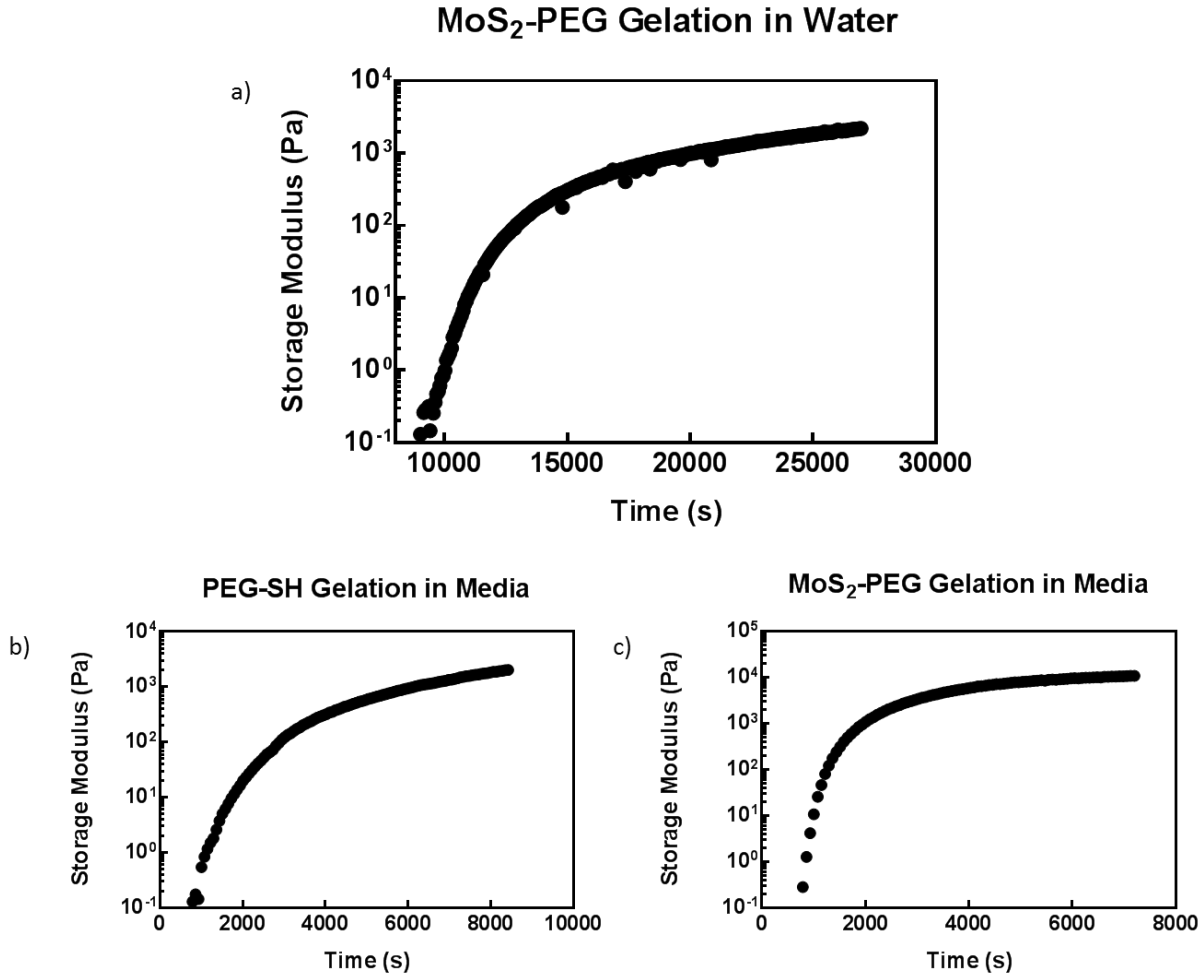

Figure 10. Gelation kinetics in different solvents. a) Gelation of MoS_2-PEG hydrogel in water occurs after a total of 24 hours. b) and c) The gelation of PEG-SH in cell culture media and the gelation of MoS_2-PEG hydrogel in media are presented respectively.

Imaging

Photographs of the prepared hydrogels can be seen in *Figure 11*. They exhibit a high enough degree of mechanical stiffness to be manipulated without deforming or breaking. *Figure 12a* shows the SEM image of a cross section of the hydrogel. Regular pores of about 10 µm can be seen throughout the gel. At the center of the pores are MoS_2 nanoassemblies. The EDS maps in *Figure 12b* illustrate the presence of MoS_2 only at the center of the pores, visually verifying that MoS_2 acts as a crosslinking agent.

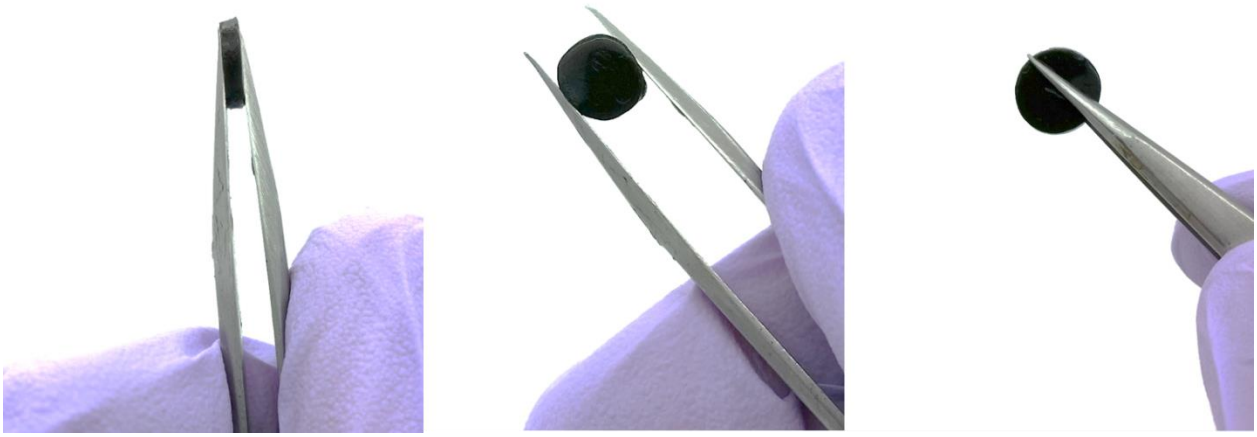

Figure 11. A swollen MoS_2-PEG hydrogel. The gels exhibit high stiffness.

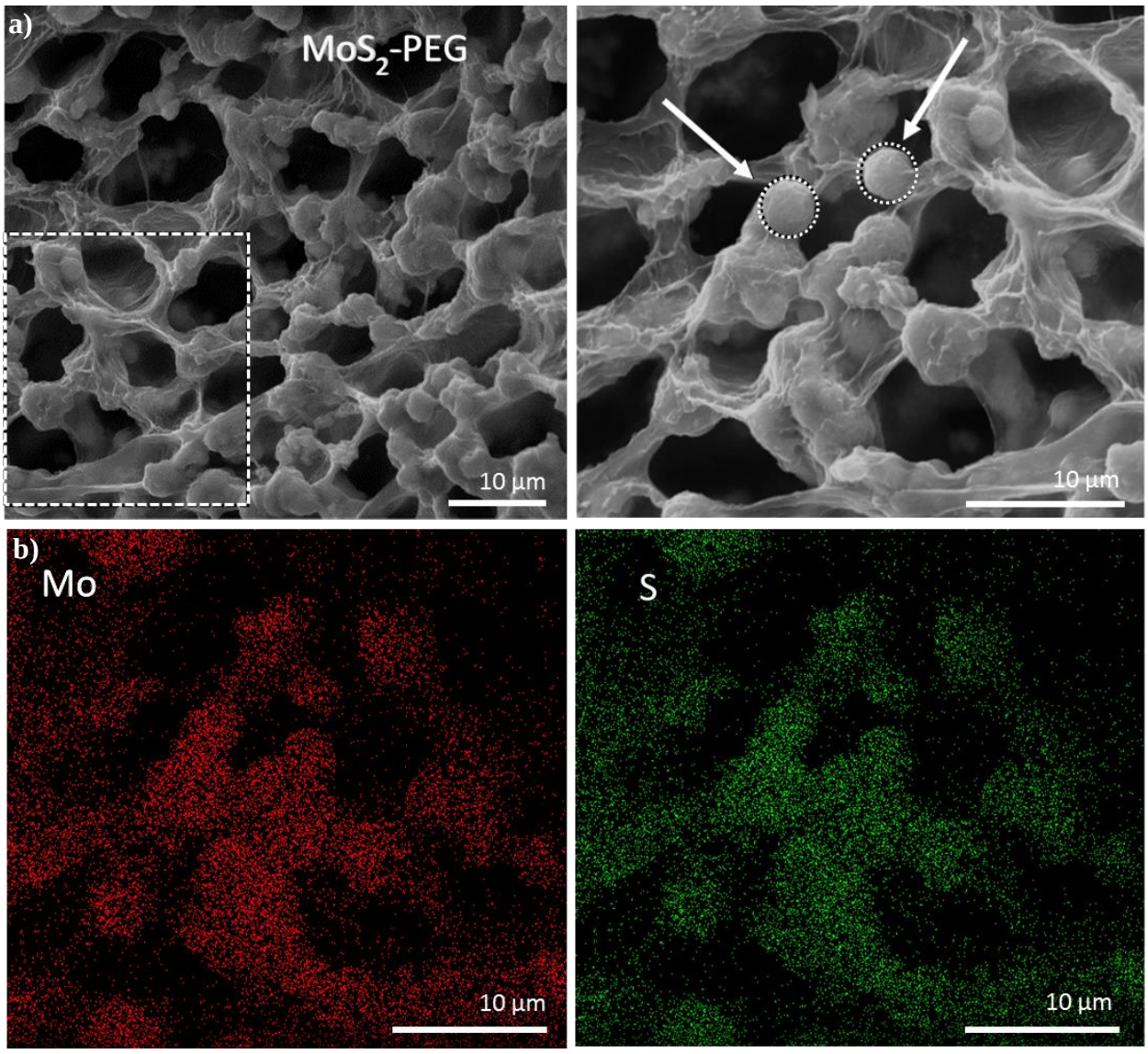

Figure 12. MoS_2-PEG hydrogel microporous structure. a) An SEM image of hydrogel pores is presented. b) EDS maps depicting spatial distributions of elemental Mo and S are presented.

Compression testing

To determine the hydrogel's viscoelastic behavior, a series of compression tests were run on multiple compositions of the hydrogel. The compressive modulus of 3 compositions were determined; as MoS_2 concentration increased, stiffness increased as seen in *Figure 13a*. *Figure 13b* depicts the energy dissipated due to hysteresis which did not follow any specific trend. The

compressive modulus (*Figure 13c*) and energy dissipated (*Figure 13d*) remained relatively constant through 4 cycles of compression for each composition, indicating good mechanical recovery.

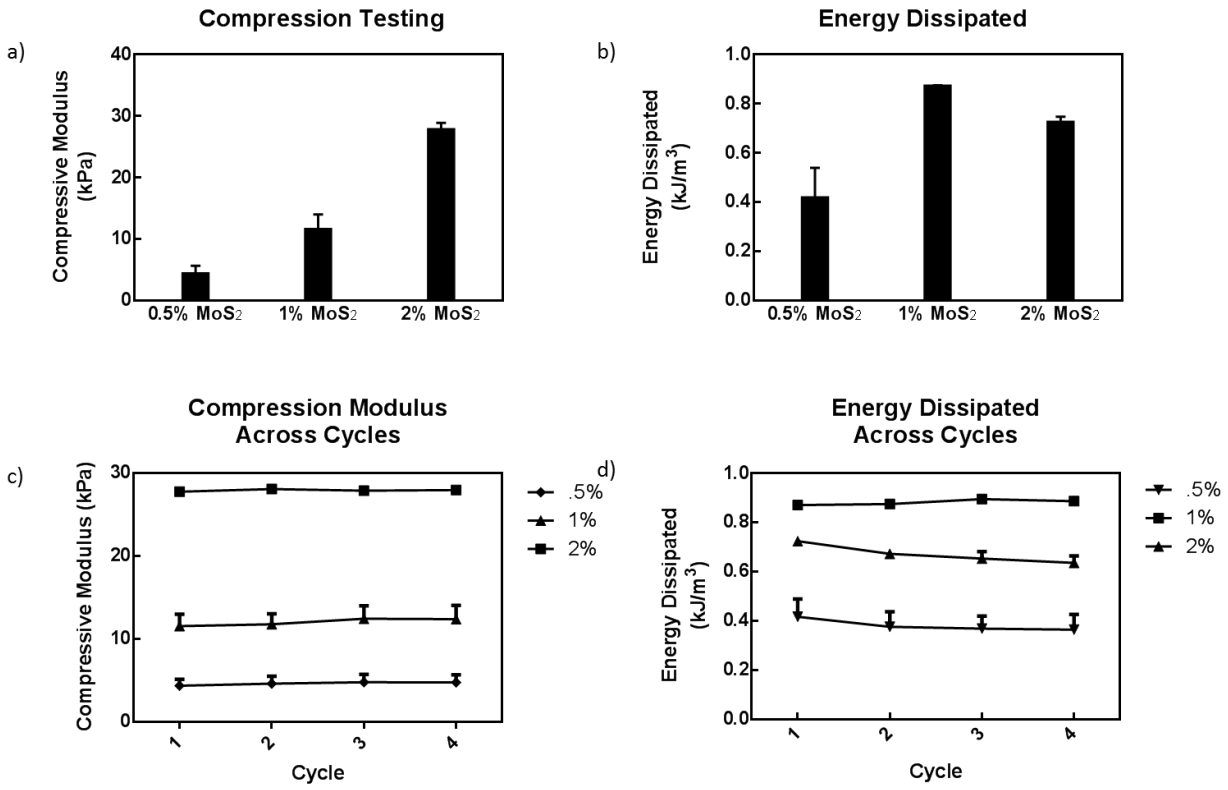

Figure 13. Viscoelastic response of the MoS_2-PEG hydrogel to uniaxial compression.

Rheological testing

To determine the hydrogel's response to shear forces, a stress sweep and frequency sweep were performed on the material. *Figure 14a* shows the response of the hydrogel to varying magnitudes of shear stress at a constant frequency of 1 Hz. The storage modulus remains at approximately 2 kPa from a range of 0.1 Pa to 13 Pa. *Figure 14b* shows the response of the

hydrogel to varying magnitudes of oscillatory frequency at a constant shear stress of 1 Pa. The storage modulus remains at approximately 2 kPa from a range of 0.1 Hz to 10 Hz.

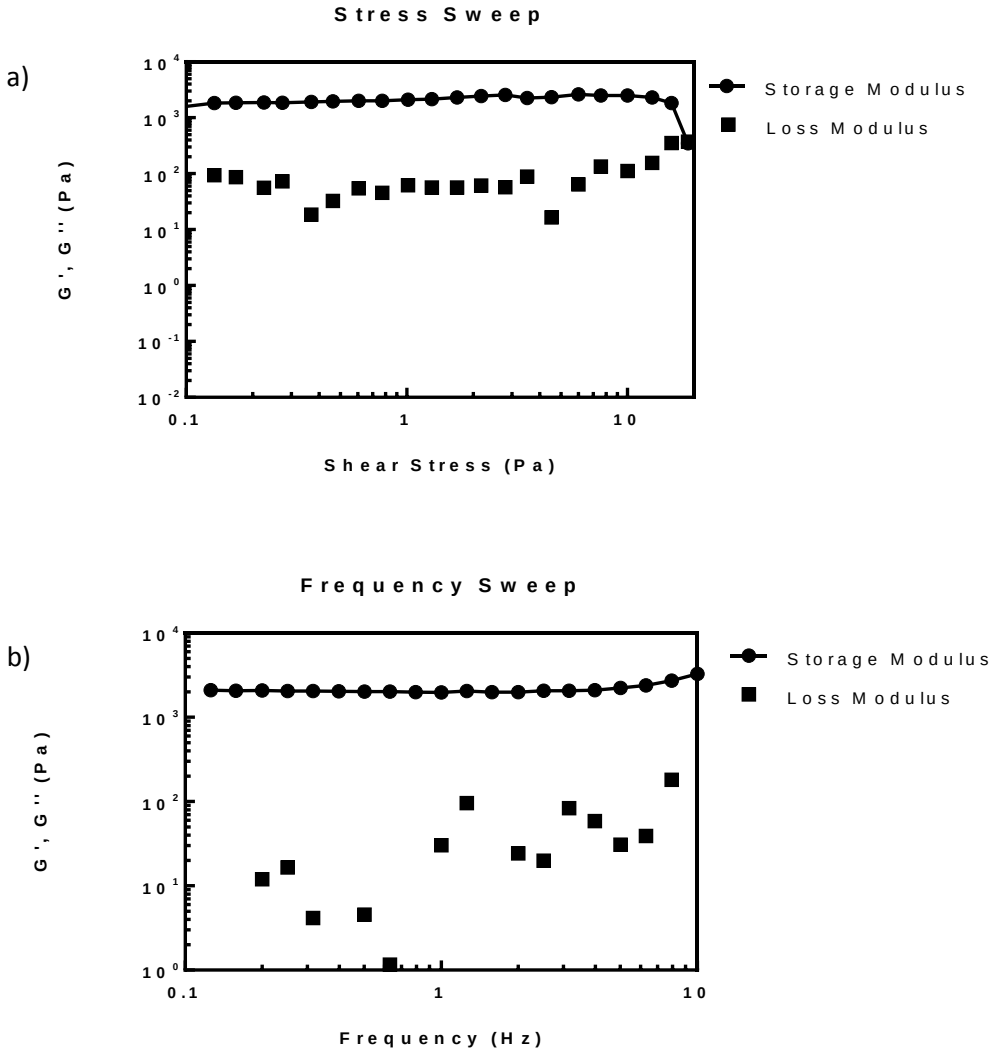

Figure 14. Viscoelastic response of the MoS_2-PEG hydrogel to oscillatory shear stress. a) The storage and loss moduli of the material are recorded from 0.1 to 20 Pa at an oscillatory frequency of 1 Hz. b) The storage and loss moduli of the material are recorded from 0.1 to 10 Hz at a shear stress of 1 Pa.

CHAPTER IV

CONCLUSION

Polymeric hydrogels play a crucial role in regenerative medicine, as they provide scaffolds for cellular encapsulation and their further differentiation in desired lineage. A catalyst-free gelation of polymers has always been sought after, as it would minimize cytotoxicity and undesirable physicochemical interactions with cells. To develop such a system, MoS_2 nanoassemblies, known for their ability to spontaneously conjugate with thiolated ligands, served as crosslink epicenters for a multi-arm PEG-SH hydrogel.

In order to promote crosslinking, defect-rich MoS_2 with abundant vacancy sites for thiol conjugation was synthesized. To optimize the gelation of the PEG-SH polymers, five different samples of defect-rich MoS_2 nanoassemblies were synthesized by varying the ratio of reactants. After characterizing the structure and defect content of each sample, it was decided that 1:4 MoS_2 was optimal for crosslinking due to its high number of defects and predominance of the 2H polytype. The resulting hydrogel showed a regular porous structure which is vital for cell proliferation, tunable viscoelastic mechanical properties that mimic those of many tissue types, and stable structural behavior throughout physiologically relevant shear oscillatory stresses. All these factors indicate that this material may be applicable for use in tissue engineering.

REFERENCES

[1] E. M. Ahmed, "Hydrogel: Preparation, characterization, and applications: A review," *J Adv Res,* vol. 6, pp. 105-21, Mar 2015.

[2] A. K. Gaharwar, N. A. Peppas, and A. Khademhosseini, "Nanocomposite hydrogels for biomedical applications," *Biotechnol Bioeng,* vol. 111, pp. 441-53, Mar 2014.

[3] J. R. Xavier, T. Thakur, P. Desai, M. K. Jaiswal, N. Sears, E. Cosgriff-Hernandez, *et al.*, "Bioactive nanoengineered hydrogels for bone tissue engineering: a growth-factor-free approach," *ACS Nano,* vol. 9, pp. 3109-18, Mar 24 2015.

[4] G. Yang, C. Zhu, D. Du, J. Zhu, and Y. Lin, "Graphene-like two-dimensional layered nanomaterials: applications in biosensors and nanomedicine," *Nanoscale,* vol. 7, pp. 14217-31, Aug 20 2015.

[5] W. Z. Teo, E. L. K. Chng, Z. Sofer, and M. Pumera, "Cytotoxicity of Exfoliated Transition-Metal Dichalcogenides (MoS2, WS2, and WSe2) is Lower Than That of Graphene and its Analogues," *Chemistry-a European Journal,* vol. 20, pp. 9627-9632, Jul 28 2014.

[6] T. Liu, C. Wang, W. Cui, H. Gong, C. Liang, X. Shi, *et al.*, "Combined photothermal and photodynamic therapy delivered by PEGylated MoS2 nanosheets," *Nanoscale,* vol. 6, pp. 11219-25, Oct 7 2014.

[7] T. Liu, C. Wang, X. Gu, H. Gong, L. Cheng, X. Shi, *et al.*, "Drug delivery with PEGylated MoS2 nano-sheets for combined photothermal and chemotherapy of cancer," *Adv Mater,* vol. 26, pp. 3433-40, Jun 4 2014.

[8] S. S. Chou, M. De, J. Kim, S. Byun, C. Dykstra, J. Yu, *et al.*, "Ligand Conjugation of Chemically Exfoliated MoS2," *Journal of the American Chemical Society,* vol. 135, pp. 4584-4587, Mar 27 2013.

[9] L. Zhou, B. Z. He, Y. Yang, and Y. G. He, "Facile approach to surface functionalized MoS2 nanosheets," *Rsc Advances,* vol. 4, pp. 32570-32578, 2014.

[10] L. Cheng, J. J. Liu, X. Gu, H. Gong, X. Z. Shi, T. Liu, *et al.*, "PEGylated WS2 Nanosheets as a Multifunctional Theranostic Agent for in vivo Dual-Modal CT/Photoacoustic Imaging Guided Photothermal Therapy," *Advanced Materials,* vol. 26, pp. 1886-1893, Mar 2014.

[11] V. Dixit, J. Van den Bossche, D. M. Sherman, D. H. Thompson, and R. P. Andres, "Synthesis and grafting of thioctic acid-PEG-folate conjugates onto Au nanoparticles for selective targeting of folate receptor-positive tumor cells," *Bioconjug Chem*, vol. 17, pp. 603-9, May-Jun 2006.

[12] Z. Kou, X. Wang, R. Yuan, H. Chen, Q. Zhi, L. Gao, *et al.*, "A promising gene delivery system developed from PEGylated MoS2 nanosheets for gene therapy," *Nanoscale Res Lett*, vol. 9, p. 587, 2014.

[13] T. Liu, S. Shi, C. Liang, S. Shen, L. Cheng, C. Wang, *et al.*, "Iron oxide decorated MoS2 nanosheets with double PEGylation for chelator-free radiolabeling and multimodal imaging guided photothermal therapy," *ACS Nano*, vol. 9, pp. 950-60, Jan 27 2015.

[14] J. Xie, H. Zhang, S. Li, R. Wang, X. Sun, M. Zhou, *et al.*, "Defect-rich MoS2 ultrathin nanosheets with additional active edge sites for enhanced electrocatalytic hydrogen evolution," *Adv Mater*, vol. 25, pp. 5807-13, Oct 25 2013.

[15] H. Nan, Z. Wang, W. Wang, Z. Liang, Y. Lu, Q. Chen, *et al.*, "Strong Photoluminescence Enhancement of MoS2 through Defect Engineering and Oxygen Bonding," *ACS Nano*, vol. 8, pp. 5738-5745, 2014/06/24 2014.